Acupuncture and Herbal Medicine

Electroacupuncture combined with cisplatin induces an effective anti-tumor immune response by protecting chemotherapy-impaired bone marrow hematopoiesis in non–small cell lung cancer mice

Jiaqi Wang[1], Yuanzhen Yang[1], Shanshan Lu[1], Jin Huang[1,2], Shanshan Li[1], Hongen Chang[1,3], Chaoyang Zhang[1], Ning Ma[4], Suhong Zhao[1,5], Shiyu Miao[1], Quynh Vo Dai[1,6], Kai Du[7], Narendra Lamichhane[1,8], Xiaohua Wen[7], Ganlu Sun[9], Yi Guo[1,9,10,11,*], Zhifang Xu[1,7,10,11,*]

[1]Research Center of Experimental Acupuncture Science, Tianjin University of Traditional Chinese Medicine, Tianjin, China; [2]Area of Regulatory Biology, Division of Life Science, Graduate School of Science and Engineering, Saitama University, Saitama, Japan; [3]The Third School of Clinical Medicine (School of Rehabilitation Medicine), Key Laboratory of Acupuncture and Neurology of Zhejiang Province, Zhejiang Chinese Medical University, Zhejiang, China; [4]Graduate School of Health Science, Suzuka University of Medical Science, Suzuka, Mie, Japan; [5]Tuina Department, Shuguang Hospital, Shanghai University of Traditional Chinese Medicine, Shanghai, China; [6]Hue Rehabilitation Hospital, Hue, Vietnam; [7]School of Acupuncture & Moxibustion and Tuina, Tianjin University of Traditional Chinese Medicine, Tianjin, China; [8]Blue Lotus Hospital, Kathmandu, Nepal; [9]School of Traditional Chinese Medicine, Tianjin University of Traditional Chinese Medicine, Tianjin, China; [10]National Clinical Research Center for Chinese Medicine Acupuncture and Moxibustion, Tianjin, China; [11]Tianjin Key Laboratory of Modern Chinese Medicine Theory of Innovation and Application, Tianjin, China

Abstract

Objective: The effectiveness of chemotherapy is affected by tumor heterogeneity and drug resistance mechanisms; however, there are certain limitations. Electroacupuncture can regulate the tumor immune response and restore bone marrow hematopoietic function, which is affected by chemotherapy. This study investigated the efficacy and mechanism of electroacupuncture combined with cisplatin in the treatment of non–small-cell lung cancer mice.

Methods: To establish a mouse model of non–small-cell lung cancer, gene sequencing combined with bioinformatics analysis, flow cytometry, and liquid-phase chips was used to observe the expression of immune cells and related factors in the mouse tumor microenvironment. Flow cytometry was used to observe subpopulations of mouse bone marrow hematopoietic stem cells and progenitor cells. PAC1 receptor agonists were used to observe mouse tumor immunity and bone marrow hematopoiesis-related indicators.

Results: The combination of electroacupuncture with high- and low-dose chemotherapy had a better tumor-suppressive effect. Electroacupuncture can affect the gene expression profile of immune cells, especially the expression levels of *Ccr1, Cxcr5*, *Zbp1*, and *Camkllα*, and increases the levels of interferon-γ (IFN-γ) and interleukin (IL)-2 protein, upregulating the levels of cytokines Ccl4, Ccl3, and IL-6 in the tumor tissue. Additionally, electroacupuncture enhanced the infiltration of $CD8^+$ T cells, dendritic cells, and M1-type macrophages at the tumor site, and reduced the proportion of Th17 and Treg cells. Furthermore, electroacupuncture remodels the bone marrow hematopoietic microenvironment after chemotherapy by increasing the number of bone marrow hematopoietic stem cell subsets, leukocytes, and subpopulations in the peripheral blood. PAC1 receptor agonists have similar effects to those of electroacupuncture on hematopoietic protection and tumor immunity after chemotherapy.

Conclusions: Electroacupuncture may improve chemotherapy-induced bone marrow suppression, reshape the tumor microenvironment immune response affected by chemotherapy, and change the tumor immune microenvironment to an anti-tumor mode by regulating tumor local immune-related cytokines. The PAC1 receptor may be a drug target for the treatment of myelosuppression and immunosuppression in patients with tumors.

Keywords: Bone marrow hematopoiesis, Cisplatin, Electroacupuncture, Immune, PACAP, Tumor microenvironment

Jiaqi Wang and Yuanzhen Yang contributed equally to this work.

**Corresponding author. Zhifang Xu, E-mail: xuzhifangmsn@hotmail.com; Yi Guo, E-mail: guoyi_168@163.com.*

Received 19 December 2024 / Accepted 27 April 2025

How to cite this article: Wang JQ, Yang YZ, Lu SS, Huang J, Li SS, Chang HG, Zhang CY, Ma N, Zhao SH, Miao SY, Vo Dai Q, Du K, Lamichhane N, Wen XH, Sun GL, Guo Y, Xu ZF. Electroacupuncture combined with cisplatin induces an effective anti-tumor immune response by protecting chemotherapy-impaired bone marrow hematopoiesis in non–small-cell lung cancer mice. Acupunct Herb Med 2025;5(2):229–245. doi: 10.1097/HM9.0000000000000158

Copyright © 2025 Tianjin University of Traditional Chinese Medicine. This is an open-access article distributed under the terms of the Creative Commons Attribution-Non Commercial-No Derivatives License 4.0 (CCBY-NC-ND), where it is permissible to download and share the work provided it is properly cited. The work cannot be changed in any way or used commercially without permission from the journal.

Introduction

Non–small-cell lung cancer (NSCLC) accounts for approximately 85% of all lung cancer cases[1]. Owing to its high incidence and challenging treatment modalities, NSCLC has become one of the main areas of focus in oncological research and clinical practice. Patients with NSCLC often experience symptoms such as cough, hemoptysis, dyspnea, and pain due to lung tumors. Symptoms such as fatigue and weight loss caused by tumor consumption severely affect patients' daily lives and psychological states, and reduce their quality of life[2]. Multimodal treatment strategies, including surgery, radiotherapy, and systemic therapy, are widely used to treat NSCLC[3]. With the advent of targeted therapies and immunotherapies, therapeutic options for NSCLC have expanded, providing new avenues for personalized and effective interventions[4–7]. Platinum-based chemotherapeutic agents remain the standard first-line treatment for patients with advanced NSCLC, either as maintenance therapy alone or in combination[8–9]. Cisplatin, one of the most commonly used platinum-based chemotherapeutic agents, induces apoptosis and cell cycle arrest by disrupting DNA replication and transcription in tumor cells[10]. It can also disrupt the characteristics of tumor stem cells and inhibit tumor recurrence and metastasis[11]. However, the emergence of cisplatin resistance and toxic side effects, such as peripheral nerve injury and myelosuppression, pose a substantial challenge to its clinical efficacy, which often leads to therapeutic failure or poor prognosis[12–16]. Additionally, cisplatin-induced myelosuppression can cause immunosuppression in the body[17]. In addition to chemotherapy, combination therapies such as targeted therapy and immunotherapy have prolonged the survival of some patients. Targeted therapy for epidermal growth factor receptor (EGFR) mutations (such as osimertinib) has shown remarkable efficacy in certain patients. However, approximately half of patients develop drug resistance during treatment[18]. Immune checkpoint inhibitors such as pembrolizumab have demonstrated good therapeutic effects in some patients. Nevertheless, the response rate to immunotherapy is relatively low in patients with EGFR mutations and anaplastic lymphoma kinase rearrangements, which restricts the treatment options for these patients[19]. The effectiveness of these therapies is influenced by tumor heterogeneity and drug resistance mechanisms. There is a lack of precise and effective predictive biomarkers to guide treatment decisions, leading to certain limitations. Therefore, it is crucial to maintain a balance between efficacy and toxicity, making the exploration of safe and effective combination therapies scientifically and clinically important to alleviate the toxicities induced by chemotherapy and enhance therapeutic efficacy.

Electroacupuncture (EA), a form of acupuncture that applies small electrical currents to acupuncture needles, exhibits potential benefits in reducing cancer-related symptoms and improving quality of life[20–23]. The American Society of Clinical Oncology and the National Comprehensive Cancer Network recommend the use of non-pharmacological interventions, such as acupuncture for the supportive treatment of cancer[24]. Clinical studies have confirmed the correlation between acupuncture, acupressure, and cancer-related pain[25]. Mechanistic studies corroborated the potential of EA in adjuvant oncology on multiple dimensions[26–31]. To improve tumor immunity, EA can increase the proportion of $CD8^+$T and natural killer (NK) cells in the tumors of mice with breast cancer to regulate inflammatory cytokines by activating the vagus nerve[27]. In addition, EA inhibits microsatellite-stable (MSS) tumor growth and increases the levels of B lymphocytes and granular enzymes. Furthermore, EA can reshape the MSS colorectal cancer tumor immune microenvironment (TIME) and render the tumor stimulator of interferon (IFN) genes dependent on programmed death-1[32]. Our previous study showed that EA combined with cisplatin had a better tumor-suppressive effect than cisplatin alone[33]. Therefore, EA has demonstrated unique advantages as an adjuvant therapy for many aspects of tumor treatment. However, mechanistic uncertainties associated with its tumor-suppressive effects have hindered its clinical use.

In an in-depth investigation of EA mechanisms to facilitate myelosuppression after chemotherapy, we found that pituitary adenylate cyclase-activating polypeptide (PACAP) and its receptor, PAC1, may be involved in the mechanism of action of EA. PACAP released from bone marrow sympathetic nerve endings promotes the proliferation of bone marrow hematopoietic stem progenitor cells (HSPCs) by binding to a specific PAC1 receptor[34]. In contrast, EA promotes the repair of bone marrow sympathetic nerves after chemotherapy in normal mice *via* the PACAP/PAC1 pathway[33]. However, whether the PACAP/PAC1 receptor also plays a role in myelopoiesis in tumor-bearing mice and influences tumor immunity remains unknown. In this study, we analyzed the mechanism by which EA assisted cisplatin to enhance anti-tumor immunity in NSCLC mice. EA improves the bone marrow hematopoietic microenvironment after chemotherapy and may regulate systemic immunity and anti-tumor immunity by improving bone marrow hematopoiesis. Additionally, the anti-tumor immunity and bone marrow hematopoietic protective function of the PAC1 agonist in a tumor environment was explored to provide a basis for acupuncture in chemotherapy potentiation combination regimens as a more attractive option. This study aims to delve deeply into the intricate immune-regulatory network underlying the treatment of EA combined with cisplatin. By leveraging the synergistic effect of EA, this approach should be integrated into the standard treatment protocol for NSCLC dominated by chemotherapy. This integration aims to reduce the premature use of targeted drugs, delay disease progression, and enhance the efficiency of medical resource utilization.

Materials and methods

Mice

Male C57BL/6 mice (n = 130, 6 weeks old, body weight 18–24 g) were obtained from Beijing Viton Lever Laboratory Animal Technology Co., Ltd. (Beijing, China; license no. SCXK [Beijing] 2016-0006). Animals were group-housed (five mice per cage) in specific

pathogen-free conditions at 25 ± 1°C with 50% to 60% humidity under a 12:12 light-dark cycle, with *ad libitum* access to standard chow diet and water. All animal experiments were performed in accordance with the NIH Guide for the Care and Use of Laboratory Animals, and the protocols were approved by the Animal Ethics Committee of the Tianjin University of Traditional Chinese Medicine (TCM-LAEC2019057). Animal welfare was monitored daily, and all efforts were made to minimize suffering, mice were acclimatized for at least 7 days before experiments.

Materials and reagents

After 1 week of loading, the mice were randomly divided into tumor (T), cisplatin (TC), and EA combined with cisplatin (TCE) groups. Cisplatin (Jiangsu Haosen Pharmaceutical Group Co., Ltd., Jiangsu, China) was dissolved in 0.9% NaCl solution at an administered dose of 3 or 5 mg/kg and intraperitoneally injected into mice in the TC and TCE groups on days 7, 10, 14, and 17. Mice in group T were intraperitoneally injected with an equal volume of 0.9% NaCl solution on the same day. The PAC1 agonist, PACAC1-38 (25 nmol/kg, i.p.; Selleck Chemicals, Houston, TX, USA), which was diluted to a concentration of 1 mmol/L using a 0.9% NaCl solution. In the afternoon of EA intervention on days 7, 9, 11, 14, 16, and 18, mice in the chemotherapy combined with PACAC1-38 (TCP) group were intraperitoneally injected with PACAP1-38, 0.2 mL/pupil, and the other groups were injected with an equal volume of saline.

Establishment of a mouse model of LLC hormonal tumors

Lewis lung carcinoma (LLC) cells (Fu Heng Biology, Shanghai, China) were recovered by rapidly thawing cryopreserved vials at 37°C, followed by centrifugation (800 rpm, 5 minutes). After discarding the supernatant, the pelleted cells were reconstituted in dulbecco's modified eagle medium containing 10% fetal bovine serum (FBS) and cultured in T-75 flasks under standard conditions (37°C, 5% CO_2). Cells can be inoculated after three to five passages, confluent cells were detached using 0.25% trypsin-ethylenediaminetetraacetic acid, neutralized with a complete medium, and centrifuged. Finally, the cells were adjusted to a concentration of 1×10^6 cells/mL for subsequent experiments. All procedures were conducted under aseptic conditions to ensure sterility. Each mouse was inoculated with 0.1 mL of 1×10^6/mL LLC cells at the right groin after disinfection. The mouse was held in a head-down and feet-up position. Keep the needle stable during slow injection, then withdraw slowly and press the site. A palpable tumor a week later indicated successful modeling. Tumors were palpable about 1 week later. On days 7, 10, 14, 17, and 21, tumor volume was measured using a Vernier caliper.

Electro-needle parameters

EA intervention was started on the same day as cisplatin treatment in the mice, and acupuncture needles were bilaterally inserted into Zusanli (ST36) (3 mm depth) and Sanyinjiao (SP6) (2 mm depth). The acupuncture needles were linked to an SDZ-V EA apparatus programmed to deliver alternating sparse-dense wave stimulation (5/25 Hz, 0.75 mA) for 15 minutes, following established protocols[33]. Animals in the TCE group underwent EA therapy at a frequency of three sessions weekly over a 14-day period, and mice in the T, TC, and TCP groups received the same soft cloth fixation, but were not EA stimulated. During the operation, acupuncture was performed strictly according to the anatomical position of the acupoints in the mice by designated individuals. The EA apparatus was calibrated and adjusted before each experiment to ensure the accuracy and consistency of EA stimulation.

Measurement of tumor growth

The longitudinal length (L) and width (W) of the tumors were measured using Vernier calipers at fixed time points on days 7, 10, 14, 17, and 21 post-loading. The tumor volume was calculated as follows: V (mm^3) = ($L \times W \times W$)/2. On day 21, the animals were anesthetized with 4% isoflurane (Shenzhen RWD Life Technology Co. Ltd, Shenzhen, China), and intact tumor tissues were removed and weighed.

Gene sequencing and data analysis

Tumor samples were extracted using the procedure described earlier and subjected to gene sequencing. The RNA was extracted and purified according to standard operating procedures. The total RNA amount and purity were determined, and the purified total RNA was subjected to mRNA sequencing library construction and sequencing. Using edgeR for inter-sample differential gene analysis, genes with fold change >1.5 were considered differentially expressed genes (DEGs). The protein–protein interaction (PPI) network was further analyzed based on the earlier results of different groups (https://cn.string-db.org/). Gene sequencing was performed using Shanghai Jikai Genetics.

Reverse transcription-quantitative polymerase chain reaction

RNA samples were quantified and validated by reverse transcription-quantitative polymerase chain reaction (RT-qPCR). Total RNA was reverse transcribed with PrimeScript RT reagent kit (Takara Bio, Kyoto, Japan), followed by amplification using SYBR Select Master Mix (Applied Biosystems, USA). Gene-specific primers (Sangon Biotech, China; Table 1) were employed, and relative expression levels were determined *via* the double-standard curve method.

Flow cytometry analysis

Bone marrow cells were collected for the HSPC subpopulation assays. The cells were detected using anti-Lin (FITC), anti-Sca-1 (PE-Cy7), anti-CD34 (APC), anti-CD16/32 (BV421), anti-CD127 (IL-7R) (BV510), anti-CD117 (cKit) (APC-Cy7), anti-CD90.1 (PerCP-Cy5.5), anti-CD135 (PE-Cy5), anti-CD135 (PE) and stained. Flow cytometric analysis was performed on an Attune NxT acoustic focusing cytometer (Thermo Fisher Scientific, Waltham, Massachusetts, USA). All

Table 1
RT-qPCR primer sequence

Genes	Forward primer (5'→3')	Reverse primer (3'→5')
Zbp1	AAGAGTCCCCTGCGATTATTTG	TCTGGATGGCGTTTGAATTGG
Itgam	ATGGACGCTGATGGCAATACC	TCCCCATTCACGTCTCCCA
Ccl5	GCTGCTTTGCCTACCTCTCC	TCGAGTGACAAACACGACTGC
18s	CGATGCTCTTAGCTGAGTGT	GGTCCAAGAATTTCACCTCT
Adra2a	GGTGTGTTGGTTTCCGTTCTTT	TAGATAACAGGGTTCAGCGAGC
Cxcl1	CACCTCAAGAACATCCAGAGCT	TTTCTGAACCAAGGGAGCTTCA
Cxcr5	TAAAGTTCCGCAGTGACCTCTC	TCTAGAAGGTGGTGAGGGAAGT
Ccr3	CACTGTACTCCCTGGTGTTCAT	GCAGGTCAGAAATTGCCAAGTT
Camk2a	ATCGCCTATATCCGCATCACTC	ATCTGTGGAAGTGGACGATCTG
C5ar1	GCCCTTATCATCTACTCGGTGG	CGCCAGATTCAGAAACCAGATG
Ccr1	TTAGCTTCCATGCCTGCCTTAT	TGAAACCTCTTCCACTGCTTCA

RT-qPCR: Reverse transcription-quantitative polymerase chain reaction.

data were analyzed as follows: positive cell events (%) = (target gate/total cell count) × 100%.

Single-cell suspensions of bone marrow were fixed in 75% ethanol at –20°C overnight. Cell samples were incubated with 0.5 mL of propidium iodide (PI; TxCyclePI/RNAse; BD Biosciences, Franklin Lakes, NJ, USA) for 15 minutes at 4°C. Analyses were performed using the ModFit 3.1 software (Verity Software, Topsham, ME, USA).

Mouse tumors were removed and single-cell suspensions of intratumor T cell, macrophage, and dendritic cell (DC) subpopulations were prepared. For the detection of T cells, the cells were incubated with anti-CD3 (FITC), anti-CD4 (PE-cy5), anti-CD8 (BV421), anti-CD45 (BV711), anti-CCR6 (BV605), anti-CCR10 (APC), anti-CXCR3 (PE), anti-CCR4 (PE-cy7), anti-CD127 (BV510), and anti-CD25 (Alexa Fluor 700). Macrophages and DC were detected using anti-CD86 (PE-cy7), anti-CD206 (Alexa Fluor 700), anti-CD11B (SB600), and anti-CD11C (PerCP-cy5.5) antibodies. The method of detection and analysis was the same as that used for the HSPCs.

Liquid chip

Luminex-xMAP technology was used to prepare tumor samples and standards for the detection of 10 cytokines: IFN-γ, interleukin (IL)-2, chemokine (C-C motif) ligand (CCL)-3, CCL4, CCL5, IL-6, IL-1α, IL-1β, tumor necrosis factor (TNF)-α, and IL-5. The experiments were conducted by Beijing Junkeyuan Technology Co.

Statistical analysis

Data are expressed as mean ± standard error of the mean. Normally distributed data were analyzed by one-way analysis of variance or repeated-measures analysis of variance. *Post-hoc* tests used least significant difference (homogeneous variance) or Dunnett's t3 (heterogeneous variance). Non-normal data employed Kruskal-Wallis test. Analyses used SPSS 23.0 ($P < 0.05$ significant). Figures were created with GraphPad Prism 9.5 (GraphPad, San Diego, CA, USA).

Results

EA combined with chemotherapy inhibited tumor growth in NSCLC mice

We observed the effect of EA combination therapy on tumor growth in NSCLC mice (Figure 1A). Tumor volume was measured in the 3 mg/kg-loaded mice using Vernier calipers on days 7, 10, 14, 17, and 21. The tumor volume of the TC and TCE groups was significantly reduced on days 14, 17, and 21 compared to that of the T group ($P < 0.01$), and that of mice in the TCE group on day 14 was statistically different from that in the TC group. On day 21, EA combined with chemotherapy decreased the tumor volume by 76% ($P < 0.01$) compared with the 45% decrease in the TC group ($P < 0.05$), indicating that TCE has a superior tumor-suppressing effect compared with TC. The weighing of the mouse tumors after sampling on day 21 revealed that the TC and TCE groups had lower tumor weights than the T group. On days 17 and 21, both the TC and TCE groups lost weight, with a more pronounced decrease in weight in the chemotherapy alone group (Figure 1B). Observation of the behavioral activity status of the mice revealed that after the first chemotherapy session, the activity of the mice in the TC and TCE groups was reduced compared to that of the T group. With an increase in the number of chemotherapy sessions, the mice's fur became less glossy, and there were no significant changes in eating and drinking. These results suggest that both cisplatin alone and EA combined with cisplatin can inhibit tumor growth in NSCLC mice and that EA may have a better potential to inhibit tumor growth after combination treatment. We wanted to determine whether EA also has a better tumor-suppressive effect at higher chemotherapy doses. Therefore, we administered a chemotherapeutic dose of 5 mg/kg to observe the anti-tumor effects of EA. Compared to the mice in the T group, the mice in the TC and TCE groups had smaller tumors on days 14, 17, and 21, and the therapeutic effect of EA in combination with chemotherapy was not better than that of the chemotherapy-only group during the overall course of tumor treatment. We weighed the tumors of the loaded mice on day 21 and found that the tumors were smaller

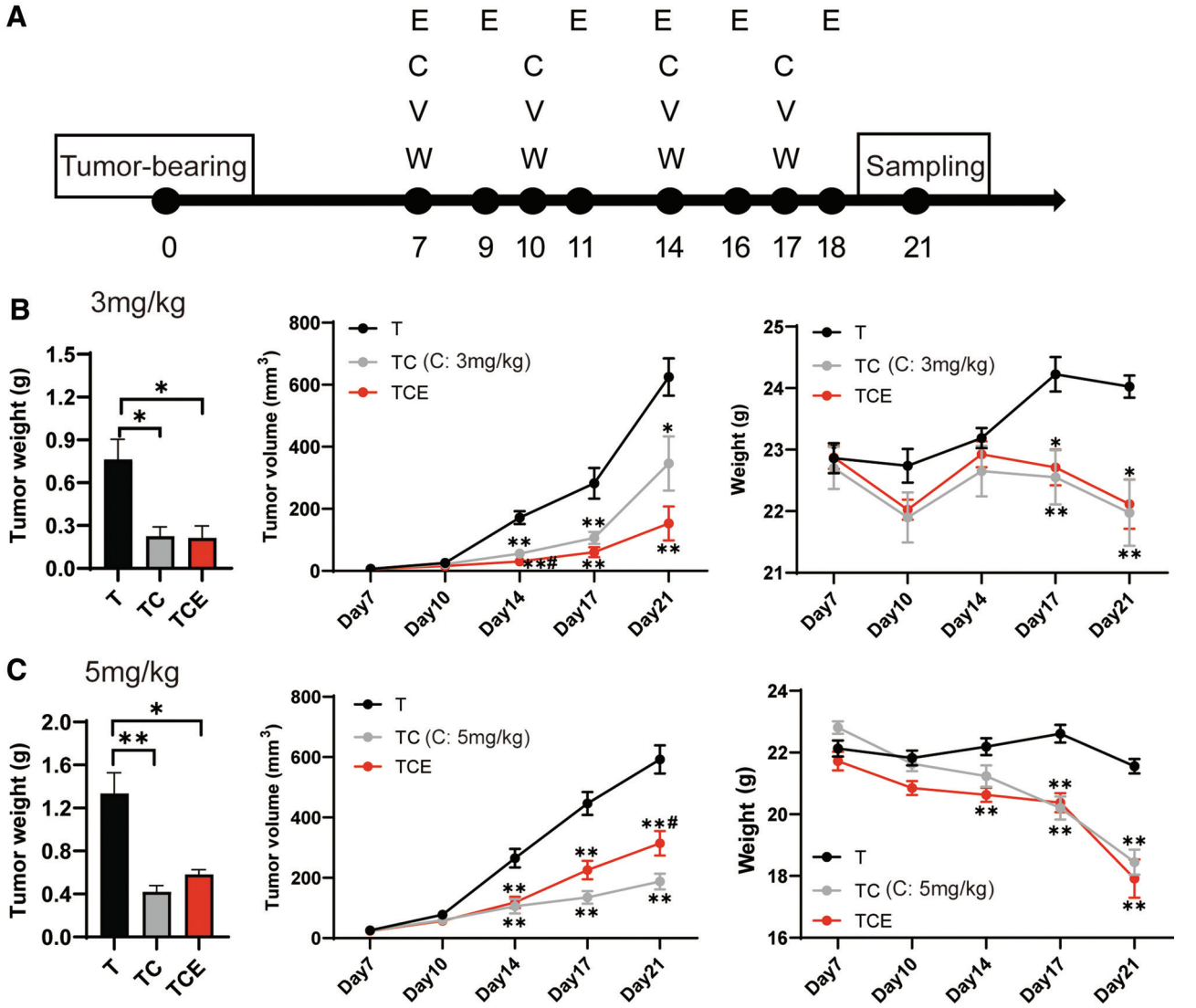


Figure 1. EA combined with low-dose chemotherapy administration reduced the tumor volume. (A) Experimental timeline for evaluating the effect of electroacupuncture (E) combined with different doses of chemotherapy (C) on tumor volume (V) and mouse body weight (W) in tumor-bearing mice. (B) Lewis Tumor mass (n = 6–10, ANOVA), low-dose cisplatin (TC, 3 mg/kg), tumor growth curves (n = 6–10, RM-ANOVA), body weight difference (n = 8, RM-ANOVA). (C) Tumor mass (n = 6–9, ANOVA), tumor growth curve (n = 9–10, RM-ANOVA), weight difference (n = 8–10, RM-ANOVA) of Lewis lung cancer mice treated with normal saline (T), high-dose cisplatin (TC, 5 mg/kg) or combined electroacupuncture (TCE) on the 21st day after tumor-bearing treatment. The above data are expressed as mean ± SEM, *P < 0.05, **P < 0.01. EA: Electroacupuncture; RM-ANOVA: repeated measures analysis of variance; SEM: standard error of the mean; T: Tumor; TC: Cisplatin; TCE: EA combined with cisplatin.

in both the TC and TCE groups than those in the T group; however, the difference was more significant in the TC group. Observation of the body weights of the mice revealed that the TCE group lost more weight than the T group on days 14, 17, and 21, and the TC group lost more weight than the T group on days 17 and 21 (Figure 1C). The behavioral activity status of the mice was consistent with that of the 3 mg/kg chemotherapy dose.

EA combined with chemotherapy modulates local tumor immune-related pathways

To explore the pathways through which EA assists low-dose chemotherapy in exerting stronger inhibitory effects on tumor growth, we screened tumor samples from each group for differential genes using RNA-seq bioinformatic analysis. Sequencing results showed 455 DEGs in the TC group compared with those in the T group, including 211 upregulated and 244 downregulated genes. Compared with the TC group, the TCE group had 356 DEGs, including 253 upregulated genes and 103 downregulated genes (Figure 2A). The expression of DEGs was consistent in each mouse group (Figure 2B). The results of the Kyoto Encyclopedia of Genes and Genomes (KEGG) pathway enrichment of DEGs in the TC group compared to the T group showed that among the top 15 KEGG-enriched pathways obtained by sorting according to the padj value, the complement and coagulation cascade, cyclic guanosine monophosphate-protein kinase G (cGMP-PKG) signaling pathway, neuroactive ligand–receptor interaction, and NK cell–mediated cytotoxicity were closely related to the immune response (Figure 2C; Table 2). Among the first 15 KEGG pathways enriched in the TCE group compared to the TC group, adrenergic signaling in cardiomyocytes, cGMP-PKG signaling pathway, neuroactive ligand–receptor interaction, complement and coagulation cascade, TNF signaling pathway, and Wnt signaling pathway were highly correlated

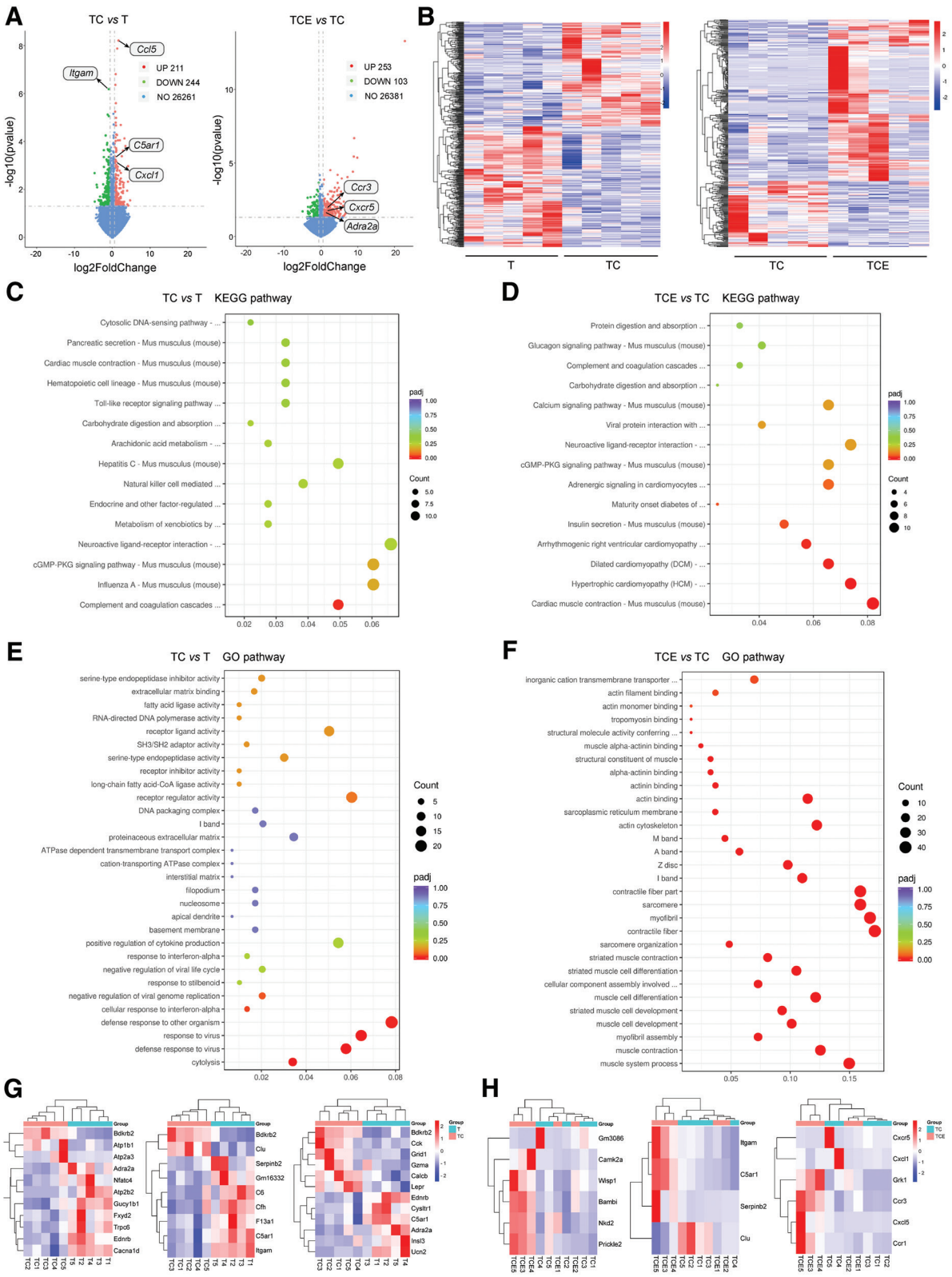


Figure 2. Gene sequencing and pathway enrichment analysis of local tumors after EA combined with low-dose chemotherapy. (A) Scatter plot of the differential gene distribution between the TC *vs.* T and TCE *vs.* TC groups. With log2 FC > 1.5 as the difference threshold, $P < 0.05$ as the significance threshold, red represents upregulated genes and green represents downregulated genes. (B) Heatmap of differential gene distribution between TC *vs.* T and TCE *vs.* TC groups, red indicates upregulation, blue indicates downregulated gene expression, and darker color represents greater difference. (C) DEG between TC *vs.* T groups, the top 15 key pathways of the resulting KEGG enrichment analysis. (D) DEG between TCE *vs.* TC groups, the top 15 key pathways from the resulting KEGG enrichment analysis. (E) DEG between TC *vs.* T groups, GO enrichment analysis of the results. (F) DEG between TCE *vs.* TC groups, and GO enrichment analysis of the results. (G) Enrichment analysis and clustering diagram of differential genes between TC group and T group in complement and coagulation cascades, cGMP-PKG signaling pathway, and neuroactive ligand–receptor interaction pathway. (H) Enrichment analysis and clustering diagram of differential genes between TCE group and TC group in complement and coagulation cascades, TNF signaling pathway, and chemokine signaling pathway. cGMP-PKG: Cyclic guanosine monophosphate-protein kinase G; DEG: Differentially expressed gene; EA: Electroacupuncture; FC: Fold change; GO: Gene Ontology; KEGG: Kyoto Encyclopedia of Genes and Genomes; T: Tumor group; TC: Cisplatin group; TCE: Electroacupuncture combined with cisplatin group; TNF: Tumor necrosis factor.

Table 2

Immune-related pathways based on KEGG and GO

(A) Focusing results of immune-related pathways in the TC group *vs.* T group based on high concentration of KEGG and GO

Description	*P* value	Count	Genes
Complement and coagulation cascades	0.00004	9	*Clu/Itgam/Bdkrb2/C5ar1/Cfh/F13a1/Serpinb2/Gm16332/C6*
cGMP-PKG signaling pathway	0.00211	11	*Bdkrb2/Ednrb/Cacna1d/Trpc6/Gucy1b1/Fxyd2/Atp1b1/Adra2a/Atp2b2/Nfatc4/Atp2a3*
Neuroactive ligand-receptor interaction	0.00457	12	*Bdkrb2/Ednrb/C5ar1/Ucn2/Lepr/Calcb/Cck/Cysltr1/Adra2a/Grid1/Insl3/Gzma*
Natural killer cell–mediated cytotoxicity	0.00904	7	*Prf1/Sh2d1a/Lat/Klra4/Gzmb/Klra7/Pik3r2*
Response to interferon-alpha	0.00005	4	*Ifit1/Ifit2/Ifit3/Ifit3b*
Regulation of T cell chemotaxis	0.00118291	3	*Ccl5/Cxcl10/Tmem102*

(B) Focusing results of immune-related pathways in the TCE group *vs.* TC group based on high concentration of KEGG and GO

Description	*P* value	Count	Genes
Adrenergic signaling	0.00212	8	*Myl3/Atp1b2/Myh7/Camk2a/Cacng1/Atp2a3/Creb3l1/Slc8a3*
cGMP-PKG signaling pathway	0.00614	8	*Atp1b2/Adra2a/Myh7/Kcnma1/Atp2a3/Ednrb/Creb3l1/Slc8a3*
Neuroactive ligand–receptor interaction	0.00690	9	*Adra2a/C5ar1/Ucn2/Gzma/Nmbr/Edn1/P2rx5/Lpar4/Ednrb*
Complement and coagulation cascades	0.02581	4	*Clu/Serpinb2/C5ar1/Itgam*
TNF signaling pathway	0.03160	5	*Cxcl5/Nod2/Edn1/Creb3l1/Cxcl1*
Wnt signaling pathway	0.03573	6	*Bambi/Camk2a/Wisp1/Prickle2/Nkd2/Gm3086*
Regulation of neutrophil chemotaxis	0.00061	6	*Cxcl5/C5ar1/Nod2/Ripor2/Edn1/Cxcl1*

cGMP-PKG: Cyclic guanosine monophosphate-protein kinase G; GO: Gene ontology; KEGG, Kyoto Encyclopedia of Genes and Genomes; T: Tumor; TC: Cisplatin; TCE: Electroacupuncture combined with cisplatin; TNF: Tumor necrosis factor.

with the immune response. Three cGMP-PKG signaling pathways, neuroactive ligand–receptor interactions, and complement and coagulation cascades, were consistent with the enrichment results in the TC group (Figure 2D; Table 2). PPI network analysis was used to identify critical regulatory nodes of these DEGs at the molecular level. The results showed that the protein products encoded by the DEGs were considerably enriched in a series of targets closely related to the TIME in both the chemotherapy and EA combination therapy groups, specifically Z-DNA binding protein 1 (Zbp1), chemokine (C-X-C motif) ligand 1 (Cxcl1), chemokine (C-C motif) receptor 1 (Ccr1), Ccr3, chemokine (C-X-C motif) receptor 5 (Cxcr5), Cxcl10, integrin alpha M (Itgam), serine peptidase inhibitor, clade B (Ovomucoid), member 2 (Serpinb2) (Figure 3A–C; Table 3). The results of both pathway enrichment and PPI network analysis suggest that chemotherapy interferes with the immune response of the local tumor microenvironment and that EA may achieve a tumor-suppressive and potentiating effect by exerting a remodeling effect on the TIME in Lewis lung cancer chemotherapy mice.

Based on the intergroup differential gene and enrichment analysis results, we verified the critical target genes in immune-related pathways using RT-qPCR. Our results showed that the expression of Ccr1, Cxcr5, Ccr3, α-2A adrenergic receptor (Adra2a) and ATPase, Na+/K+ Transporting, β 2 Polypeptide (Atp1b2) decreased in the tumor after chemotherapy; Itgam and calcium/calmodulin-dependent protein kinase II α (CamkIIα) showed a decreasing trend compared with the T group; and *Zbp1* and *Cxcl1* were unchanged compared with the tumor group. The content of *Ccr1, Cxcr5, Zbp1,* and *CamkIIα* genes rebounded after the increase of EA. The expression of the *Cxcl1* gene in the TCE group was significantly lower than that in the TC group. The expression of *Itgam* and *Adra2a* genes showed no statistical difference compared to that in the TC group. However, their levels decreased compared to those in the tumor group after chemotherapy. In contrast, there was a tendency for expression to increase after EA, as was the trend of changes in other immune-related genes in the present experiment. Meanwhile, there was a trend of increased *Ccl5* gene expression after increasing the EA dose compared with that in the TC group. It still did not affect *Ccr3* gene expression (Figure 3D). The above results verified the gene sequencing results, showing that the local tumor immune environment shifted toward a pro-tumor environment to a certain extent after chemotherapy. Therefore, EA upregulated the expression of local anti–tumor-related genes.

EA combined with chemotherapy recruited immune effector cells into the tumor microenvironment by modulating local tumor immune-related cytokines

Based on the earlier RNA-seq enrichment analysis and validation results, we deduced that EA may remodel the chemotherapy-affected TIME *via* immunochemotaxis and improve the anti-tumor ability of local immune cells in the lesion to achieve tumor suppression. To confirm our hypothesis, we used flow cytometry to compare the percentages of various types of local tumor immune cells in multiple groups. We analyzed the numbers of local M1 macrophages ($CD11b^+$ $CD86^+$), M2 macrophages ($CD11b^+$ $CD11c^+$), and DCs ($CD11B^+$ $CD206^+$) in the tumors. Compared to the tumor group, EA combined with chemotherapy increased the number of local DCs by 83% and M1 macrophages by 32% ($P < 0.05$). However, there was no statistically significant

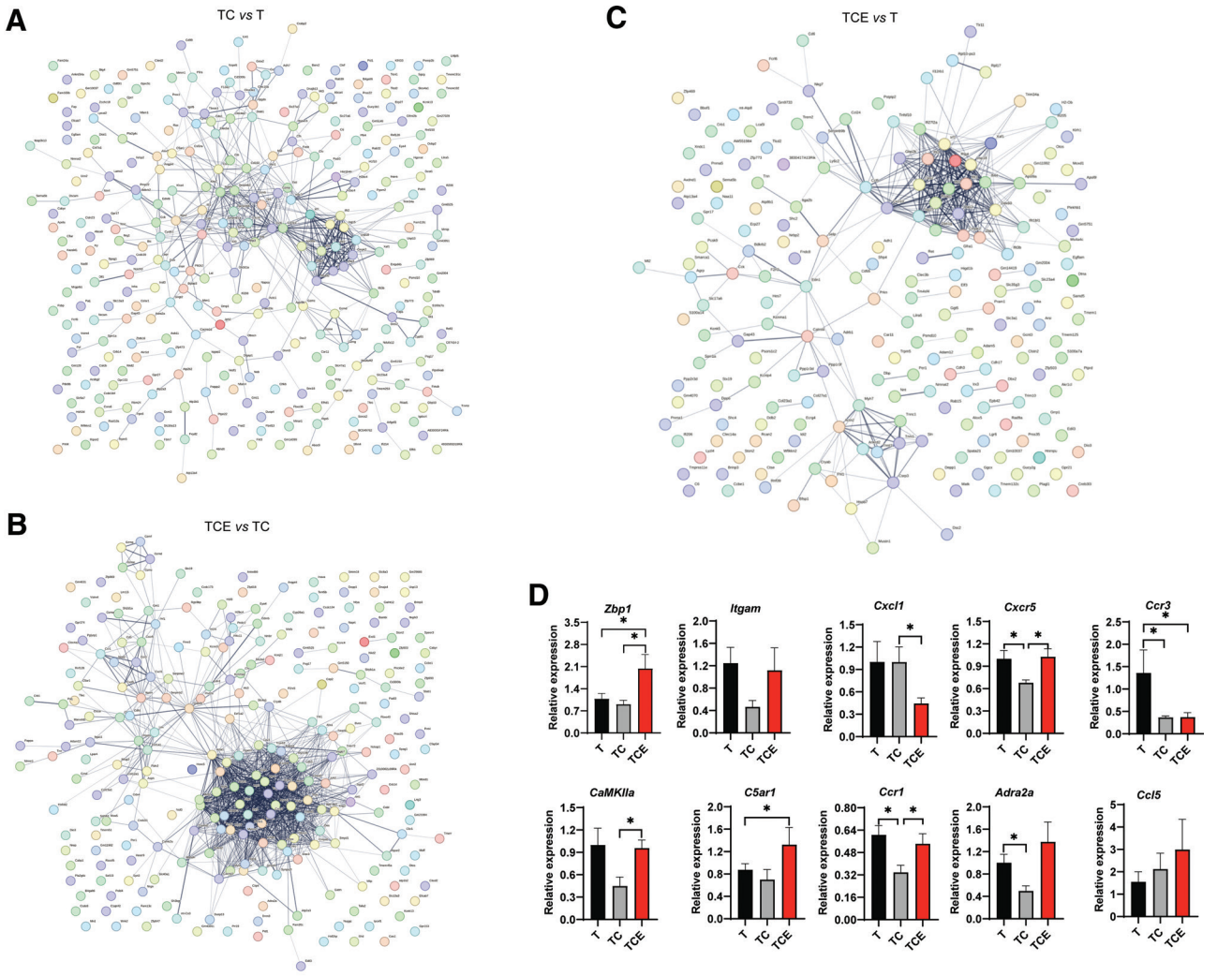


Figure 3. Effect of EA combined with low-dose chemotherapy on the expression levels of genes associated with anti-tumor immune cells in tumor tissues. (A) Analysis plot of the PPI interaction based on the DEG results between the TC *vs.* T groups. (B) Analysis plot of the PPI interaction based on the DEG results between the TCE *vs.* TC groups. (C) Analysis plot of the PPI interaction based on the DEG results between the TCE *vs.* T groups. (D) Expression levels of immune cell–related genes screened based on KEGG, GO enrichment analysis, and PPI network interaction analysis (n = 6, 7, ANOVA, Kruskal-Wallis test). These data are presented as the mean ± SEM, with *P < 0.05. ANOVA: analysis of variance; DEG: Differentially expressed gene; EA: Electroacupuncture; FC: Fold change; GO: Gene ontology; KEGG: Kyoto Encyclopedia of Genes and Genomes; PPI: Protein–protein interaction; SEM: standard error of the mean; T: Tumor group; TC: Cisplatin group; TCE: Electroacupuncture combined with cisplatin group.

difference in the number of M2 macrophages among the three groups after EA combined with chemotherapy (Figure 4A, B). Therefore, EA may activate local innate immune responses in tumors. We further focused on the effect of EA on the local adaptive immune response in tumors. We found that the number of $CD8^+$ T cells in the TIME decreased by 27% after chemotherapy, and the number of local $CD8^+$ T cells in the tumor increased by 84% after an increase in EA compared to that in the TC group ($P < 0.05$). Different cytokines regulate $CD4^+$ T cells and differentiate in different directions, thereby mediating different types of immune responses. Chemotherapy alone or in combination with EA did not significantly affect the overall number of $CD4^+$ T cells. The number of Th17 cells was significantly lower in the TCE group than in the T and TC groups, and the number of Tregs in the TCE group was 29% lower than that in the T group (Figure 4C, D). To precisely explore how EA achieves its remodeling effect on the proportion of immune cells in the TIME after chemotherapy, we measured the content of critical cytokines for information exchange between local immune cells in tumors using Luminex-xMAP liquid-phase microarray technology and found that the majority of upregulated inflammatory factors were associated with the activation of the T cell immune response after EA combined with chemotherapy intervention. Compared to the T group, the TCE group showed an increase in the content of CCL4 protein, which plays the role of chemotactic T cells, NK cells, and macrophages, by 31%, and chemotherapy alone increased it by 17%. EA combined with chemotherapy had a more significant effect in enhancing the content of CCL4, a local chemokine in the tumor, than the chemotherapy-only group ($P < 0.05$, TC *vs.* T; $P < 0.01$, TCE *vs.* T). Only the combination therapy resulted in an increase in the local tumor content of IFN-γ and IL-2, which are involved in the proliferation and activation of T cells ($P < 0.05$ TCE *vs.* T). Compared to the TC group, EA combined with chemotherapy increased local Ccl3 and IL-6 levels (Figure 4E). Based on the role of these cytokines in promoting the immune response of T cells, it was hypothesized that increased EA intervention might

Table 3

Protein number and frequency of PPI high nodes among the three groups

(A) Protein and frequency of high PPI nodes in the TC and T groups

Node	Node degree	Node	Node degree	Node	Node degree	Node	Node degree
Cxcl10	32	*Rsad2*	19	*Tlr8*	17	*Oas3*	16
Itgam	32	*Serpinb2*	18	*Apol9a*	16	*Serpinb1a*	16
Ccl5	29	*Usp18*	18	*Cd163*	16	*Serpinb8*	16
Irf7	21	*Csf1r*	17	*Gbp3*	16	*Serpinb9b*	16
Isg15	21	*Ifit1*	17	*Ifi44*	16	*Cxcr5*	15
Prf1	21	*Ifit2*	17	*Il33*	16	*Fgf7*	15
Gzmb	20	*Ifit3*	17	*Itga2*	16	*Cmpk2*	14

(B) Protein and frequency of high PPI nodes in the TCE *vs.* TC groups

Node	Node degree	Node	Node degree	Node	Node degree	Node	Node degree
Itgam	21	*Jph2*	16	*Lox*	13	*Edn1*	11
Myo18b	21	*Eef1a2*	15	*Mybph*	13	*Trim72*	11
Myom3	20	*Postn*	15	*Smyd1*	13	*Cdh1*	10
Hspb7	19	*Abra*	14	*Synpo2l*	13	*Fhl1*	10
Ampd1	18	*Cryab*	14	*L09Rik*	12	*Serpinb2*	10
Des	18	*Cxcl1*	13	*Prf1*	12	*Ccr1*	8
Art1	16	*Cxcr5*	13	*Stac3*	12	*Sypl2*	8

(C) Protein and frequency of high PPI nodes in the TCE *vs.* T groups

Node	Node degree	Node	Node degree	Node	Node degree	Node	Node degree
Cxcl10	26	*Ifit1*	24	*Oas3*	20	*Cmpk2*	17
Irf7	26	*Usp18*	24	*Ccl5*	19	*Apol9a*	16
Ifi44	25	*Ifit2*	23	*Oas1g*	19	*Gbp2b*	16
Ifit3	25	*Rsad2*	23	*Rtp4*	19	*Zbp1*	16
Isg15	25	*Oas2*	21	*Ddx60*	18	*Xaf1*	15

PPI: Protein–protein interaction; T: Tumor; TC: Cisplatin; TCE: Electroacupuncture combined with cisplatin.

achieve tumor suppression by influencing a variety of T cell-related immune cytokines in the tumor after chemotherapy and promoting the anti-tumor immune response of T cells.

EA combined with chemotherapy remodels the bone marrow hematopoietic microenvironment

Considering that local tumor immunity relies on a constant supply of peripheral blood, the improvement of local tumor immunity after chemotherapy by EA found in the above studies, and the fact that EA can improve bone marrow hematopoiesis by repairing bone marrow sympathetic nerves, we focused on the intermediate association between the TIME and peripheral blood hematopoiesis in an immune cell population. The total peripheral blood leukocyte count decreased by 25% and the lymphocyte counts decreased by 28% after chemotherapy. After increasing the EA dose, peripheral leukocytes and lymphocytes rebounded, and neutrophils and monocytes significantly increased compared to those in the T and TC groups (Figure 5A), in which monocytes acted as precursor cells for the differentiation of DC and macrophages. This suggests the possibility of anti-tumor immune cell infiltration into the TME.

Several studies have shown that chemotherapy can lead to various side effects, including myelosuppression and neurotoxicity, accompanied by significant peripheral blood lymphocyte DNA damage and induction of apoptosis in peripheral blood lymphocytes. Flow cytometry was used to analyze specific HSPC subsets in the bone marrow to further observe changes in bone marrow hematopoiesis in the cancerous state. HSPCs (markers are shown in Figure 5B) are predominantly located in the bone marrow and can give rise to cells of all hematopoietic lineages. HSPCs are divided into long-term HSCs (LT-HSPCs) and short-term HSPCs (ST-HSPCs), with LT-HSPCs differentiating into ST-HSPCs, which subsequently differentiated into multipotent progenitor cells (MPPs). Differentiation occurs in a hierarchical sequence, giving rise to common lymphoid progenitors with lymphoid potential (CLPs), or common myeloid progenitors with myeloid, erythroid, and megakaryocytic potentials (CMPs). CMPs differentiate into granulocyte-macrophages (GMPs) and megakaryocyte-erythroid progenitors (MEPs). In the next stage, GMPs differentiate into granulocytes/monocytes, and MEPs generate megakaryocytes/erythrocytes. Another type of CLPs comprised dendritic T, B, and NK cells (Figure 5B). Analysis of various bone marrow

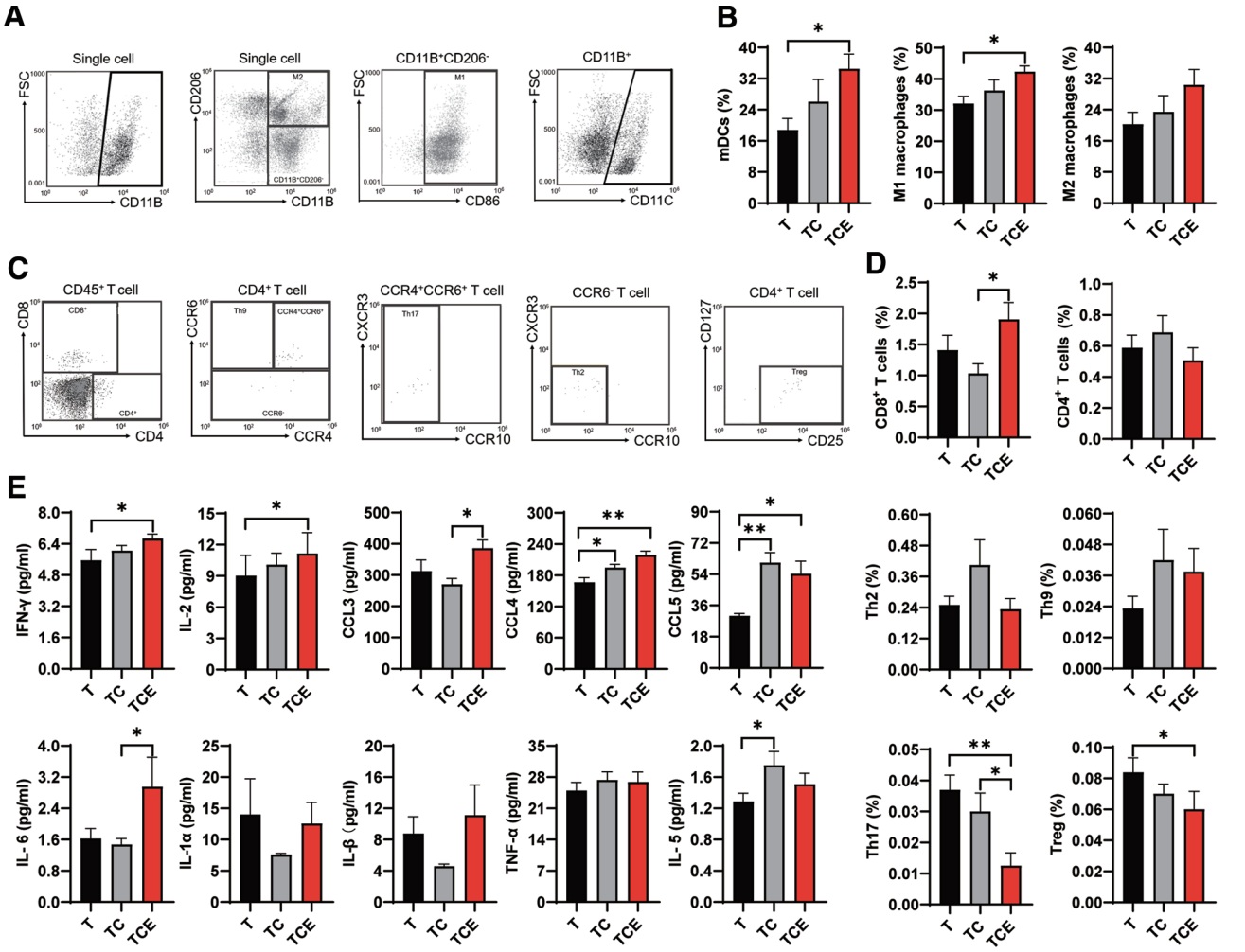


Figure 4. EA combined with low-dose chemotherapy can improve local anti-tumor immune cell infiltration. (A) Representative flow diagram and box selection scheme of tumor local myeloid immune cells. (B) Percentages of local M1 and M2 macrophages and DCs in each mouse group (n = 9, 10, ANOVA, Kruskal-Wallis test). (C) Representative flow diagram and box selection of immune cells in local lymphoid tumor lymphoid lines. (D) Percent of local T cell subsets in each group (n = 8–10, ANOVA). (E) Local immune-related cytokines in each group (n = 5, 6, ANOVA, Kruskal-Wallis test). The above data are presented as mean ± SEM, *P < 0.05, **P < 0.01. ANOVA: analysis of variance; DC: Dendritic cell; EA: Electroacupuncture; SEM: standard error of the mean; T: Tumor group; TC: Cisplatin group; TCE: Electroacupuncture combined with cisplatin group.

HSPC subpopulations revealed that the number of HSPCs, LT-HSPCs, and ST-HSPCs in the bone marrow, particularly LT-HSPCs, decreased after chemotherapy. The number of MPPs differentiated from ST-HSCs and their downstream CLPs and GMPs decreased, whereas the numbers of MEPs and CMPs remained unchanged. The number of MPPs and their downstream CMPs and CLPs significantly increased after a 2-week EA intervention at ST36 and SP6 (Figure 5C, E), and the differentiation of these cells produced numerous daughter hematopoietic cells, which maintained the stability of the hematopoietic system and preserved normal myelopoietic function.

The distribution of the bone marrow cell cycle may reflect the state of bone marrow proliferation. We observed the cell cycle profiles of bone marrow cells using PI nuclear staining. EA maintained normal cell proliferation by increasing the proportion of G2 M-phase and G2 M + S-phase bone marrow cells (Figure 5D, F). Fourteen days of EA treatment increased the number of bone marrow cells in the synthesis and division phases and protected bone marrow hematopoietic function in mice with lung cancer, which may be an essential basis for influencing relevant immune effectors in the tumor microenvironment.

Role of PAC1 receptor in remodeling the bone marrow hematopoietic microenvironment and improving tumor immunity by EA combined with chemotherapy

Multiple physiological actions of PACAP are mediated by its binding to different G protein-coupled receptors, including PAC1, vasoactive intestinal peptide receptor (VPAC) 1, and VPAC2[35]. Our previous study showed that sympathetically released PAC1 receptors mediate the EA-induced amelioration of cisplatin-induced leukopenia in normal mice[33]. To investigate whether the PACAP/PAC1 target could also provide an advantage for the myelopoietic protective effects of EA during chemotherapy in the tumor setting, we separately injected NSCLC chemotherapeutic mice with intraperitoneal PAC1 agonists for 2 weeks and performed tumor growth studies in loaded tumor mice, including tumor growth curves, immune cell infiltration, and bone marrow analyses using flow cytometry. The results showed that exogenous PAC1 agonists could potentially limit

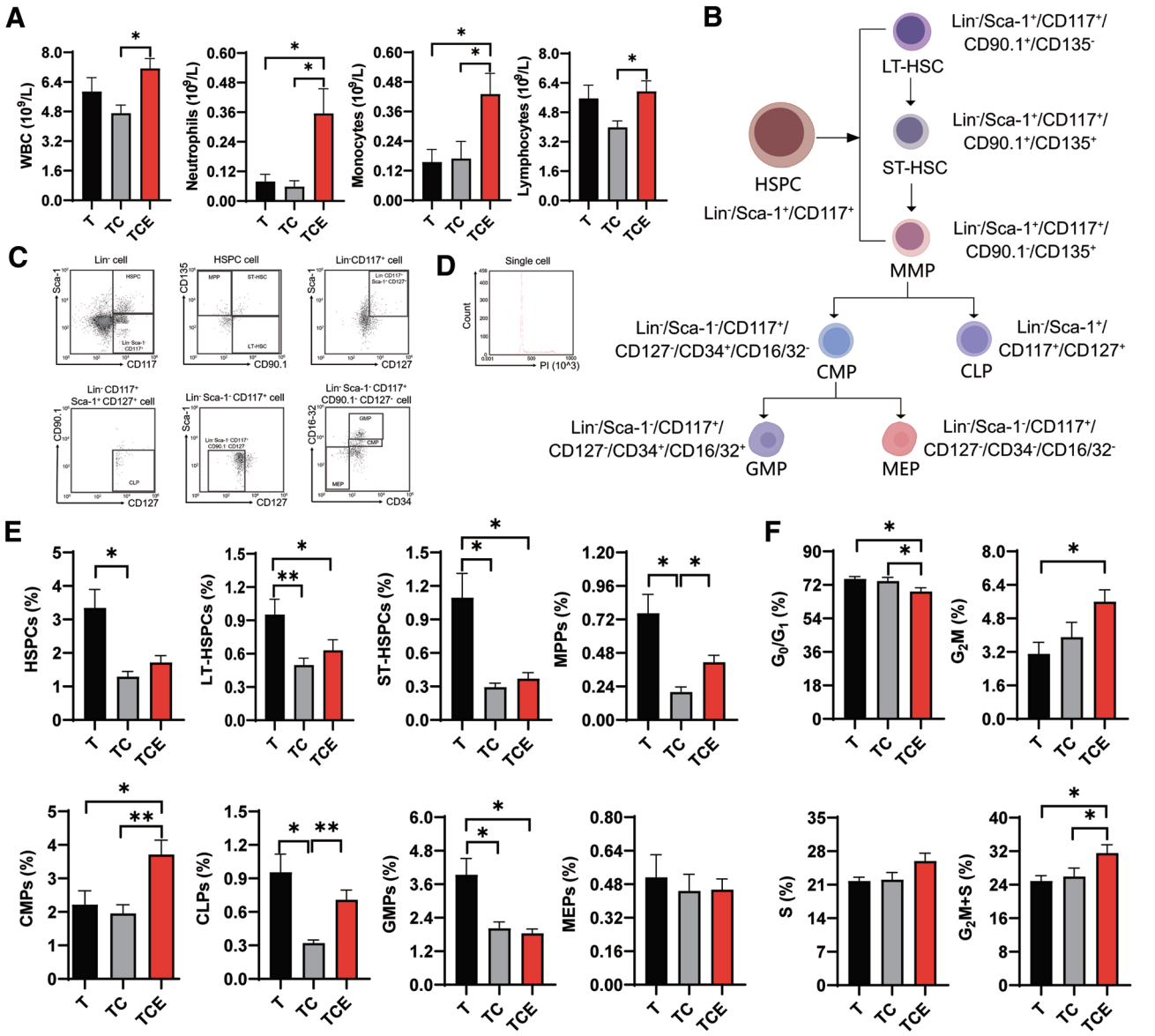


Figure 5. EA combined with low-dose chemotherapy can improve bone marrow hematopoiesis and improve peripheral immunity. (A) Number of peripheral blood leukocytes, neutrophils, monocytes, and lymphocytes in the blood of Lewis lung cancer mice in each group (n = 8–10, ANOVA, Kruskal-Wallis test). (B) The differentiation process of bone marrow hematopoietic stem cells. (C) Representative flow diagram and box selection scheme of bone marrow hematopoietic stem cells of Lewis lung cancer mice. (D) Representative flow diagram of the bone marrow cell cycle in Lewis lung cancer mice. (E) Percentage of hematopoietic stem progenitors in Lewis lung cancer mice in each group (n = 8, 9, ANOVA). (F) Percentage of bone marrow cell cycle in Lewis lung cancer mice in each group (n = 7–10, ANOVA). The above data are presented as mean ± SEM, *P < 0.05 and **P < 0.01. ANOVA: analysis of variance; CLP: Lymphoid potential; CMP: Megakaryocytic potential; EA: Electroacupuncture; GMP: Granulocyte-macrophages; HSPC: Hematopoietic stem progenitor cell; LT-HSPC: Long-term HSPC; MEP: Megakaryocyte-erythroid progenitors; MPP: Multipotent progenitor cell; SEM: standard error of the mean; ST-HSPC: Short-term HSPCs; WBC: White blood cell.

tumor growth in NSCLC mice on day 17 compared to the chemotherapy-only group, with a significant difference on day 21. Tumor weights were significantly lower than those in the tumor chemotherapy group on day 21, which was consistent with the trend of tumor suppression by EA (Figure 6A, B). We assessed the role of PAC1 receptors at the level of the TIME, and PAC1 receptor agonists similarly increased the number of local tumor M1 macrophages, DCs, and $CD8^+$ T cells, and found that the number of Th17 cells decreased after chemotherapy (Figure 6C, D). Similar to EA, the PAC1 receptor agonist PACAP1-38 restored the number of MPPs and GMPs after chemotherapy, providing a partial source of HSC replenishment and the possibility of maintaining the function of the immune system after chemotherapy, but with a reduction in the number of LT-HSPCs (Figure 6E). Therefore, PAC1 receptors may be partially involved in the reestablishment of bone marrow hematopoietic system function after chemotherapy and may mediate the role of EA in protecting myelopoietic function after chemotherapy in NSCLC mice.

Discussion

In this study, we investigated the effects of EA on tumor growth and its potential mechanisms of action. The Lewis lung cancer mouse model was used, with the TC group as a control, based on the equivalent dose ratio of 70 kg standard adult body weight converted to 20 g mouse body surface area[36]; 3 mg/kg was used as a low-dose

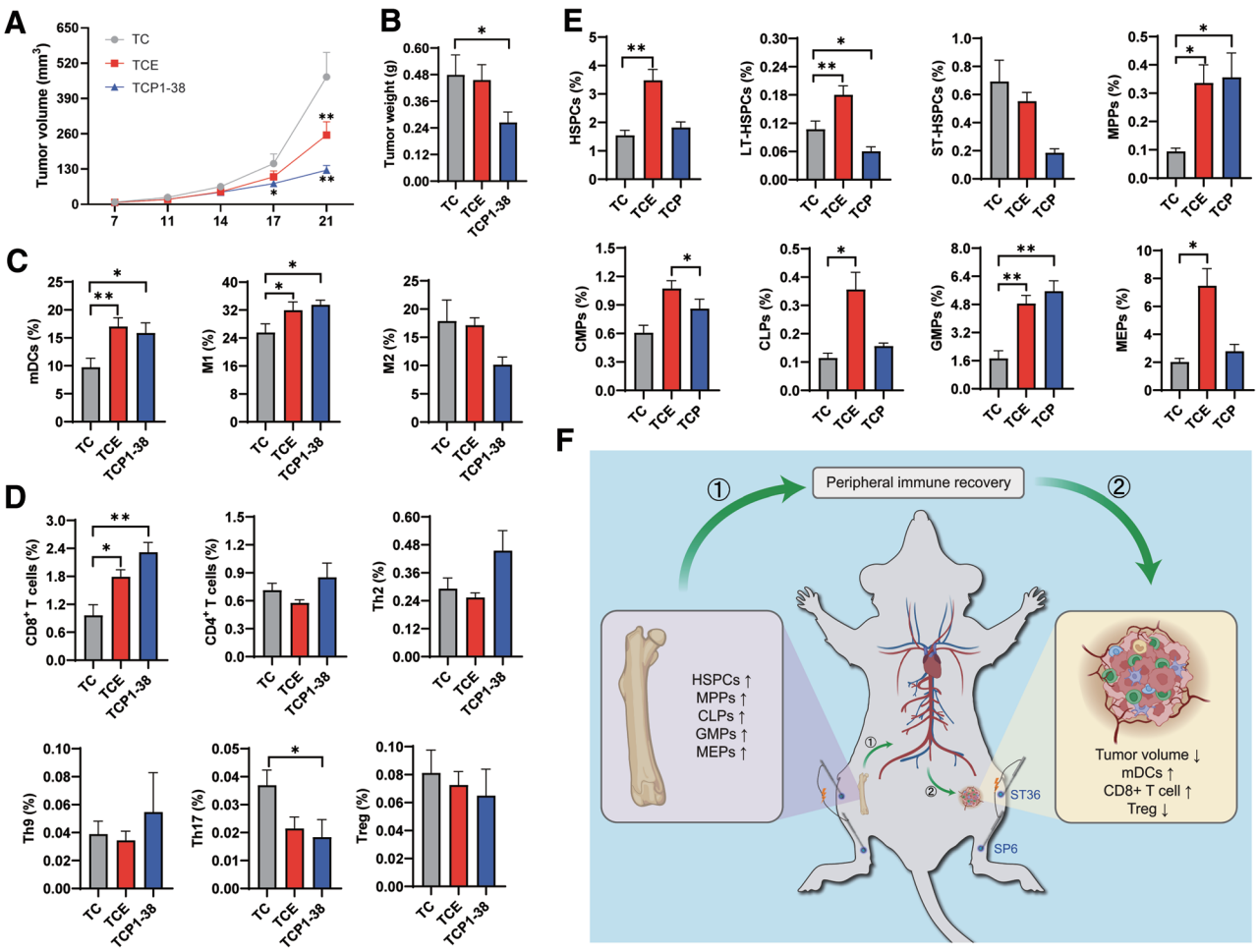


Figure 6. The PAC1 receptor pathway is involved in the EA regulation of immune cell subset infiltration in tumor tissues. (A) Tumor growth curves of lung cancer mice in each group after low-dose cisplatin administration. Tumor volumes were calculated by vernier calipers at days 7, 10, 14, 17, and 21 after tumor-bearing (n = 9–10, RM-ANOVA). (B) Lewis Tumor mass (n = 8, ANOVA) in lung cancer mice treated with low-dose cisplatin (TC, 3 mg/kg), combined with EA (TCE), or combined with PAC1 receptor agonist (TCP). (C) Percentage of local M1 and M2 macrophages and dendritic cells in each mouse group (n = 8, ANOVA, Kruskal-Wallis test). (D) Percent of local T cell subsets in mice (n = 6–10, ANOVA). (E) The percentage of bone marrow HSPC subsets in Lewis lung cancer mice in each group (n = 6, ANOVA, Kruskal-Wallis test). (F) Mechanism of tumor suppression achieved by electroacupuncture to improve immunosuppression after low-dose chemotherapy. The above data are presented as mean ± SEM, *P < 0.05 and **P < 0.01. ANOVA: analysis of variance; CLP: Lymphoid potential; CMP: Megakaryocytic potential; EA: Electroacupuncture; GMP: Granulocyte-macrophages; HSPC: Hematopoietic stem progenitor; LT-HSPC: Long-term HSPC; MEP: Megakaryocyte-erythroid progenitors; MPP: Multipotent progenitor cell; SEM: standard error of the mean; ST-HSPC: Short-term HSPCs; T: Tumor group; TC: Cisplatin group; TCE: Electroacupuncture combined with cisplatin group.

chemotherapy intervention and 5 mg/kg as a high-dose chemotherapy parameter in lung cancer mice. The effects of high- and low-dose chemotherapeutic agents on the TIME were also investigated. Both 3 and 5 mg/kg chemotherapy and EA combination therapy reduced the tumor volume in hormone-treated mice, with the EA combination therapy group exhibiting better efficacy. The overall status of mice improved with 3 mg/kg chemotherapy. However, EA at a dose of 5 mg/kg did not show a better effect than chemotherapy. Clinical studies have demonstrated that low-dose cisplatin administration is associated with a lower risk of moderate-to-severe toxicity than a high-dose cyclic administration regimen[37]. Considering that low-dose metronomic chemotherapy exhibits better clinical tumor-suppressing effects and has gradually become an alternative to traditional high-dose single-chemotherapy[38], we focused on whether EA can demonstrate a better "synergistic effect" under an optimal chemotherapy regimen (low-dose intervention) and also better simulate the clinical dosing regimen. In addition, we referred to several basic studies on the toxicity and side effects of chemotherapy and found that 3 mg/kg was the commonly selected experimental dose of cisplatin[39–40]. Therefore, most of the experiments in this study used low-dose chemotherapy (3 mg/kg). However, chemotherapy parameters vary in different tumor models, and the diversity of experimental conditions may lead to differences in experimental results in terms of efficacy and immunomodulation. Thus, it is necessary to conduct systematic evaluations using multiple tumor models and different chemotherapy strategies in the future to ensure the universality of the research results.

Low-frequency EA had a better therapeutic effect than high-frequency EA[41]. Therefore, an EA frequency of 5 Hz was selected. Considering that the body may gradually adapt to a single-frequency electrical stimulation pattern over long-term use, resulting in a gradual weakening of the stimulation effect, we adopted a dense-sparse wave pulse waveform, which alternately outputs low-frequency (5 Hz) and high-frequency (25

Hz) waves to ensure the continuity and stability of the treatment effect. Considering the tolerance of the mice, we chose an EA intensity of 0.75 mA to avoid obvious stress responses in the mice when the intensity was too high. In clinical practice, the single treatment time for EA is generally 15 to 30 minutes. Prolonged EA stimulation in mice leads to fatigue and excessive stress responses. Combined with the good treatment effect of 15 minutes of EA on cisplatin-treated mice in our previous research, we used a single EA treatment duration of 15 minutes in this study.

We focused on the tumor microenvironment to elucidate the potential mechanism by which EA reduces toxicity and increases chemotherapeutic efficacy in mice with Lewis lung cancer. We evaluated the changes in the local immune microenvironment after chemotherapy. Chemotherapy acts on tumor cells and reduces lesions while exerting different degrees of inhibitory effects on other normal cells in the body, which may create an environment more conducive to the survival of tumor cells[42]. A clinical study of TIME changes in patients with advanced gastric cancer before and during platinum-based chemotherapy revealed that some patients did not respond to chemotherapy. The expression of the immunosuppressive receptor LAG3 on the surface of T cells increases and the number of local DC in the tumor abruptly decreases[43]. Another cellular experiment focused on the effects of cisplatin and carboplatin on 10 different types of cervical and ovarian cancer cell lines and found that cisplatin or carboplatin treatment increased the ability of tumor cells to induce IL-10-secreting M2-type macrophages, and the chemotherapy-mediated increase in tumor-promoting M2 macrophages may be one of the mechanisms contributing to chemoresistance[44]. Our study found that *Ccr1*, *Cxcr5, Ccr3,* and *Adra2a* expression decreased in tumors after chemotherapy, while *Zbp1* and *Cxcl1* were essentially unchanged compared to those in the T group. *Cxcr5*, which is expressed on $CD8^+$ T cells, promotes aspects of granzyme B, TNF-α, and IFN-γ production[45]. *Adra2a* induces an anti-tumor immune response[46], and chemotherapy suppresses anti-tumor immunity to a certain extent.

We further observed changes in the TIME after the addition of EA to chemotherapy. We found that the *Ccr1*, *Cxcr5, Zbp1*, and *CamkIIα* rebounded, and the expression of *Cxcl1* decreased after increasing EA. *Cxcl1* inhibits reactive oxygen species-scavenging enzyme activity, enhances the sensitivity of tumors to radiation therapy, and participates in the chemotaxis of myeloid-derived suppressor cells (MDSCs) toward tumor convergence, inducing chemoresistance[47]. Activation of *Zbp1* enhances DC antigen cross-activation and increases $CD8^+$ T cell infiltration[48]. CaMKIIa is the major isoform of CaMKII that promotes Beclin 1 ubiquitination and autophagy in neuroblastoma cells[49]. Analysis of immune cells and related cytokines showed that EA combined with chemotherapy increased the number of tumor local DC and M1 macrophages, and increased IFN-γ and IL-2 cytokines, which are secreted by activated T cells and have anti-tumor effects, compared to those in the T group. EA also increased the number of $CD8^+$ T cells, which declined in the TIME after chemotherapy, and increased the tumor local IL-6 content. As myeloid antigen-presenting cells, DC and macrophage subpopulations induce antigen-specific immune responses by acquiring, processing, and presenting antigens to naïve T cells[50]. DCs release inflammatory cytokines as innate immune responsive cells, which play an essential role in the suppression of tumor growth and act as messengers between the innate and adaptive immune systems. The antigen cross-presentation pathway expresses tumor antigen-processing products on the cell surface as antigenic peptide-major histocompatibility complex class I molecular complexes with cytotoxic effects on $CD8^+$ T cells[51–52]. Endogenous IFN-γ protects the host from growth and primary chemo induction of transplanted tumors and hinders spontaneous tumor formation. Immunogenic fibrosarcomas grow faster in mice treated with an IFN-γ-specific neutralizing monoclonal antibody *via* tumor grafts[53]. Experiments based on a 3-methylcholanthrene-induced tumor formation model revealed shortened tumor latency in knockout mice[54]. Our results corroborate that EA may be involved in the activation of antigen presentation by DCs to $CD8^+$ T cells, which remodel the TIME by activating local intrinsic or adaptive immune responses. This suggests that the combination of EA and chemotherapy can further converge the TIME toward anti-tumor effects by regulating local immune-related cytokines.

The host immune status significantly affects the TIME and influences tumor progression, treatment response, and overall prognosis. Our study demonstrated the effects of EA on the immune status of mice undergoing chemotherapy for tumors. By observing the number of immune cells in the peripheral blood, it was found that EA increased the number of leukocytes, neutrophils, monocytes, and lymphocytes in the peripheral blood after chemotherapy, which activated the systemic immune status, providing the possibility for immune cells to localize and migrate toward the tumor and lift its immune-suppressive state. The bone marrow is the largest hematopoietic factory that differentiates into various mature blood cells and generates multiple immune system cells. A previous study found that EA on ST36 and SP6 could prevent cisplatin-induced neurotoxicity and immunosuppression, and protect bone marrow hematopoietic function[33]. Our current study observed that EA increased the number of myeloid-originating cell populations, CMPs, and progenitor cell populations, CLPs, in the bone marrow hematopoietic cell populations, as well as the number of immune effector cells (macrophages) and DCs in the tumor. EA may promote the differentiation of immature myeloid cells to mature immune cells and have a specific immune effector orientation for the differentiation of immune cells in the tumor, which may be the basis for the improvement of the immune environment after EA. Hematopoietic stem/progenitor cells in the bone marrow and peripheral blood can differentiate into immature myeloid cells and migrate to different peripheral organs, where they differentiate into mature immune cells, such as macrophages, DCs, and granulocytes, and exert immune functions. However, in the cancerous state, these immature myeloid cells are affected by tumor-derived factors and are unable to further differentiate into mature hematopoietic cells, thus remaining at their

respective stages of differentiation and becoming a class of highly heterogeneous immunomodulatory cells, that is, MDSCs, which not only inhibit the proliferation and functional activity of T cells and lead to tumor immune tolerance but are also directly involved in the development of tumor stemness, angiogenesis, stromal formation, and epithelial-to-mesenchymal transition, thereby promoting tumor growth and metastasis[55]. Maintaining normal bone marrow hematopoiesis helps to maintain a sufficient quantity and quality of HSCs, which supports faster recovery of hematopoiesis after chemotherapy and radiotherapy, reduces the risk of treatment-associated anemia and infections, helps patients better tolerate the treatment dose, reduces the likelihood of interruptions and dose adjustments, and therefore improves the outcome of the treatment and patient survival rate.

PACAP plays a vital role in bone marrow hematopoiesis; previous studies have found that sympathetic nerves promote the proliferation of bone marrow HSPCs *via* PACAP and EA improves leukopenia after chemotherapy *via* the PACAP/PAC1 pathway[34]. Peripheral immune cells and immunomodulatory molecules that continuously circulate throughout the body *via* the blood and lymphatic systems serve as crucial links between the site of the primary tumor and the host's immune organs. Simultaneously, as a blood supply to the primary tumor, they directly provide cellular and molecular components to the tumor microenvironment[56]. Traditionally, tumor immunology has mainly focused on the local immune status within the tumor microenvironment. However, the immune response itself is coordinated across tissues, and the occurrence of local anti-tumor immunity must be based on continuous communication with peripheral immune cells[57]. Considering the damage caused by chemotherapy to the body's immune system, this study further explored whether EA and PAC1 receptor agonists, while alleviating post-chemotherapy peripheral immunosuppression, also have a synergistic effect on the local immune remodeling of tumor tissues and inhibition of tumor growth. Specifically, EA may improve bone marrow hematopoietic function through the PACAP/PAC1 pathway, thereby correcting the post-chemotherapy peripheral immune deficiency, restoring the levels of peripheral immune cells, and subsequently improving the local immune supply to tumors. This also aids in the transformation of the TIME toward an anti-tumor pattern. This process may involve the anti-tumor remodeling effects of EA or PAC1 agonists on the post-chemotherapy TIME.

Our results showed that injection of the PAC1 agonist significantly inhibited tumor growth and increased the number of MPPs and GMP cells in bone marrow hematopoiesis, which was consistent with the expected results. PAC1 agonists increase the number of $CD8^+$ T cells, DCs, and M1 macrophages in the TIME. These results suggested a role for the PACAP/PAC1 receptor pathway in tumor hematopoiesis and immunity, similar to that of EA. In combination with the previously identified role of the PACAP/PAC1 pathway in mediating the EA-induced improvement of bone marrow hematopoiesis by EA in cisplatin-prone mice, we hypothesized that the PACAP/PAC1 pathway may also be involved in the inhibition of tumor growth by EA in combination with chemotherapy in LLC mice. Further studies are required to elucidate its mechanism of action. Undeniably, the systemic administration of PAC1 agonists demonstrated a better synergistic effect than EA in a Lewis lung cancer mouse model and showed more substantial advantages in reducing tumor weight. This also suggests that, in addition to participating in improving bone marrow hematopoiesis and influencing local tumor immune delivery, the PACAP/PAC1 receptor pathway may be involved in immune remodeling of the TIME directly or indirectly through other pathways. Because tumors are innervated by abnormally excited sympathetic nerves, some studies have proposed that the immunoprotective effect of PACAP is based on its neuromodulatory effect on sympathetic neurons[58]. The improvement of nerve function in a hypoxic tumor environment by activating the PACAP/PAC1 pathway may be a target for the direct regulation of the tumor microenvironment. Other studies have found that in glioblastoma, PACAP inhibits the activity of hypoxia-inducible factors by regulating the PI3K/AKT and MAPK/ERK pathways, thereby interfering with the hypoxic microenvironment[59]. Additionally, *in vitro* experiments have shown that PACAP interferes with hypoxia or angiogenesis by reducing the release of vascular endothelial growth factor and inhibiting the formation of vessel-like structures[60]. Improving the hypoxic state of tumors to assist in anti-tumor immunity may also be one of the key mechanisms through which the PACAP/PAC1 receptor pathway exerts its effects on tumors. Thus, drugs targeting the activation of local PAC1 receptors in NSCLC tumors are also worthy of further research and development and may assist in targeted and precise tumor treatment. This study confirms the role of EA in lifting immunosuppression and protecting bone marrow hematopoiesis after chemotherapy and corroborates the advantages of EA combined with chemotherapy in enhancing the anti-tumor immune response and improving anti-tumor efficacy, which provides a safer and more practical option for the combined treatment strategy of tumors.

Compared to traditional immunomodulatory therapy, EA has a unique mechanism of action in tumor treatment, which focuses on regulating the homeostasis of the tumor microenvironment and inducing the orderly release of endogenous factors. In this study, we found that EA may improve the TIME by affecting the gene expression profile of immune cells, increasing the infiltration of immune effector cells into the local tumor, protecting the hematopoietic function of the bone marrow after chemotherapy, and remodeling the hematopoietic microenvironment of the bone marrow. However, the anti-tumor mechanisms of EA remain unclear. In breast cancer murine models, EA improved the hypoxic TME by reducing microvessel density, increasing pericyte coverage, and promoting vascular normalization, thereby inhibiting tumor cell proliferation[61]. Furthermore, EA enhances the efficiency of chemotherapeutic drug delivery and reduces drug resistance[26]. Clinical evidence from multicenter trials ($n = 249$) has indicated the efficacy of EA in improving quality-of-life indices and alleviating treatment-related symptoms in patients[62–66]. However, clinical translation faces challenges because of inconsistent treatment protocols and limited large-scale

randomized controlled trials. While short-cycle high-frequency EA may induce adaptive fatigue, long-cycle low-frequency EA protocols often fail to maintain immune activation. These limitations underscore the need for standardized protocols and rigorous clinical validation.

This study has some limitations. We only observed the changes in bone marrow hematopoietic stem cell subsets and TIME after EA, and further exploration is needed to explore the correlation between bone marrow hematopoiesis and tumor immunity after EA. We observed similar effects of PAC1 receptor agonists and EA, but whether PAC1 receptors are involved in the process by which EA improves bone marrow hematopoiesis and tumor immunity requires further verification. The long-term protective effects of EA on bone marrow hematopoiesis require further research with an extended observation period. This study focused on the peripheral mechanism underlying the anti-tumor effect of EA; its central mechanism needs to be further explored. In our study, we focused on the indicators of tumor volume and body weight; however, changes in the behavioral activity status of mice after chemotherapy and EA need to be further quantified to evaluate the safety and effectiveness of chemotherapy and EA. When studying immune cell populations in the tumor microenvironment, it is necessary to comprehensively observe the expression levels of surface markers on various immune cells within the tumor microenvironment to assess dynamic changes of cells and the interactions between them.

EA holds great promise as an adjuvant treatment for tumors. Future research should focus on multicenter, large-sample, randomized controlled trials with rigorous designs to evaluate EA's efficacy, safety, and impact of EA on quality of life when combined with cisplatin in NSCLC treatment. Further investigations of EA in combination with emerging immunotherapies are essential. Combining basic research, the anti-tumor effects of different EA acupoint combinations and stimulation parameters in combination with immunotherapies should be compared to screen the optimal combination regimen and break through the bottleneck of a single therapy. Based on individual differences such as the patient's tumor type, tumor stage, physical condition, and immune status, personalized EA combined treatment regimens should be explored to determine the optimal EA treatment cycle and frequency that considers both efficacy and patient compliance, maximizing the therapeutic benefits of EA.

Conclusion

The present study demonstrates that EA and chemotherapy inhibit tumor growth in a mouse model of Lewis lung cancer. EA may selectively affect the relevant immune effector cell progenitors in the tumor microenvironment by remodeling the bone marrow hematopoietic microenvironment after chemotherapy and shifting the TIME towards an anti-tumor mode through the recruitment and activation of anti-tumor immune cells by local cytokines in the lesion. This study also found that PAC1 receptor agonists have similar effects on EA in tumor hematopoiesis and immunity, and may be candidate modulators of the role of EA in the tumor environment.

Conflict of interest statement

The authors declare no conflict of interest.

Funding

This work was supported by the National Key Research and Development Program of China (2022YFC3500404), the Natural Science Foundation of China (NSFC) (81704146, 82205310), the Research Program Project of Tianjin Education Commission (2021KJ120), and the National College Student Innovation and Entrepreneurship Training Program (202410063009).

Author contributions

Zhifang Xu and Yi Guo conceived the project. Jiaqi Wang, Yuanzhen Yang, Shanshan Lu, Jin Huang, Chaoyang Zhang, Hongen Chang, Quynh Vo Dai, and Narendra Lamichhane performed the experiments. Jiaqi Wang, Yuanzhen Yang, Shanshan Li, Suhong Zhao, Shiyu Miao, and Ganlu Sun performed the data analysis. Zhifang Xu, Yi Guo, Kai Du, Xiaohua Wen, Ning Ma provided administrative, technical, or material support. Jiaqi Wang and Yuanzhen Yang analyzed data, organized data presentation, and completed manuscript writing and preparation. Zhifang Xu reviewed and edited. All authors contributed to the article and approved the submitted version.

Ethical approval of studies and informed consent

The experimental procedures were approved by the Tianjin University of Traditional Chinese Medicine Animal Research Committee (TCM-LAEC2019057).

Acknowledgments

None.

Data availability

The datasets generated during and/or analyzed during the current study are available from the corresponding author on reasonable request.

References

[1] Leiter A, Veluswamy RR, Wisnivesky JP. The global burden of lung cancer: current status and future trends. *Nat Rev Clin Oncol* 2023;20(9):624–639.
[2] Hendriks LE, Kerr KM, Menis J, et al. Non-oncogene-addicted metastatic non-small-cell lung cancer: ESMO Clinical Practice Guideline for diagnosis, treatment and follow-up. *Ann Oncol* 2023;34(4):358–376.
[3] Gridelli C, Rossi A, Carbone DP, et al. Non-small-cell lung cancer. *Nat Rev Dis Primers* 2015;1:15009.
[4] Meador CB, Hata AN. Acquired resistance to targeted therapies in NSCLC: updates and evolving insights. *Pharmacol Ther* 2020;210:107522.
[5] Khalifa J, Amini A, Popat S, et al.; International Association for the Study of Lung Cancer Advanced Radiation Technology Committee. International association for the study of lung cancer advanced radiation technology committee. Brain metastases

from NSCLC: radiation therapy in the era of targeted therapies. *J Thorac Oncol* 2016;11(10):1627–1643.
[6] Leonetti A, Assaraf YG, Veltsista PD, et al. MicroRNAs as a drug resistance mechanism to targeted therapies in EGFR-mutated NSCLC: current implications and future directions. *Drug Resist Updat* 2019;42:1–11.
[7] Huang D, Tang Z, Pu X, et al. A novel cabazitaxel liposomes modified with ginsenoside Rk1 for cancer targeted therapy. *Acupunct Herbal Med* 2024;4(1):113–121.
[8] Saw S, Ong BH, Chua K, et al. Revisiting neoadjuvant therapy in non-small-cell lung cancer. *Lancet Oncol* 2021;22(11): e501–e516.
[9] Goldstraw P, Ball D, Jett JR, et al. Non-small-cell lung cancer. *Lancet* 2011;378(9804):1727–1740.
[10] Romani A. Cisplatin in cancer treatment. *Biochem Pharmacol* 2022;206:115323.
[11] Johnstone TC, Suntharalingam K, Lippard SJ. The next generation of platinum drugs: targeted Pt(II) agents, nanoparticle delivery, and Pt(IV) prodrugs. *Chem Rev* 2016;116(5):3436–3486.
[12] Mollman JE. Cisplatin neurotoxicity. *N Engl J Med* 1990;322(2):126–127.
[13] Getaz EP, Beckley S, Fitzpatrick J, et al. Cisplatin-induced hemolysis. *N Engl J Med* 1980;302(6):334–335.
[14] Pabla N, Dong Z. Cisplatin nephrotoxicity: mechanisms and renoprotective strategies. *Kidney Int* 2008;73(9):994–1007.
[15] Brock PR. New insights into cisplatin ototoxicity. *Cancer* 2022;128(1):43–46.
[16] Stewart JD, Bolt HM. Cisplatin-induced nephrotoxicity. *Arch Toxicol* 2012;86(8):1155–1156.
[17] Xu G, Chen H, Wu S, et al. Eukaryotic initiation factor 5A2 mediates hypoxia-induced autophagy and cisplatin resistance. *Cell Death Dis* 2022;13(8):683.
[18] Le X, Puri S, Negrao MV, et al. Landscape of EGFR-dependent and -independent resistance mechanisms to osimertinib and continuation therapy beyond progression in EGFR-mutant NSCLC. *Clin Cancer Res* 2018;24(24):6195–6203.
[19] Lee A, Nagasaka M. CheckMate-722: the rise and fall of nivolumab with chemotherapy in TKI-refractory EGFR-mutant NSCLC. *Lung Cancer (Auckl)* 2023;14:41–46.
[20] Mao JJ, Liou KT, Baser RE, et al. Effectiveness of electroacupuncture or auricular acupuncture vs usual care for chronic musculoskeletal pain among cancer survivors: the PEACE randomized clinical trial. *JAMA Oncol* 2021;7(5):720–727.
[21] Epstein AS, Liou KT, Romero S, et al. Acupuncture vs massage for pain in patients living with advanced cancer: the IMPACT randomized clinical trial. *JAMA Netw Open* 2023;6(11):e2342482.
[22] Garland SN, Xie SX, DuHamel K, et al. Acupuncture versus cognitive behavioral therapy for insomnia in cancer survivors: a randomized clinical trial. *J Natl Cancer Inst* 2019;111(12):1323–1331.
[23] Hershman DL, Unger JM, Greenlee H, et al. Effect of acupuncture vs sham acupuncture or waitlist control on joint pain related to aromatase inhibitors among women with early-stage breast cancer: a randomized clinical trial. *JAMA* 2018;320(2):167–176.
[24] Swarm R, Anghelescu DL, Benedetti C, et al. Adult cancer pain. *J Natl Compr Canc Netw* 2007;5(8):726–751.
[25] He Y, Guo X, May BH, et al. Clinical evidence for association of acupuncture and acupressure with improved cancer pain: a systematic review and meta-analysis. *JAMA Oncol* 2020;6(2):271–278.
[26] Yang M, Wan Y, Jiang X, et al. Electro-acupuncture promotes accumulation of paclitaxel by altering tumor microvasculature and microenvironment in breast cancer of mice. *Front Oncol* 2019;9:576.
[27] Zhang Z, Yu Q, Zhang X, et al. Electroacupuncture regulates inflammatory cytokines by activating the vagus nerve to enhance antitumor immunity in mice with breast tumors. *Life Sci* 2021;272:119259.
[28] Wang N, Zhao L, Zhang D, et al. Research progress on the immunomodulatory mechanism of acupuncture in tumor immune microenvironment. *Front Immunol* 2023;14:1092402.
[29] Xu X, Feng X, He M, et al. The effect of acupuncture on tumor growth and gut microbiota in mice inoculated with osteosarcoma cells. *Chin Med* 2020;15:33.
[30] Kun L, Zhu B. Significance of pleasant touch and state-of-the-art neuroscience technologies in acupuncture research. *Acupunct Herbal Med* 2023;3(1):55–58.
[31] Guo Y, Li Y, Xu T, et al. An inspiration to the studies on mechanisms of acupuncture and moxibustion action derived from 2021 Nobel Prize in Physiology or Medicine. *Acupunct Herbal Med* 2022;2(1):1–8.
[32] Wang Y, Liu F, Du X, et al. Combination of anti-PD-1 and electroacupuncture induces a potent antitumor immune response in microsatellite-stable colorectal cancer. *Cancer Immunol Res* 2024;12(1):26–35.
[33] Li S, Huang J, Guo Y, et al. PAC1 receptor mediates electroacupuncture-induced neuro and immune protection during cisplatin chemotherapy. *Front Immunol* 2021;12:714244.
[34] Xu Z, Ohtaki H, Watanabe J, et al. Pituitary adenylate cyclase-activating polypeptide (PACAP) contributes to the proliferation of hematopoietic progenitor cells in murine bone marrow via PACAP-specific receptor. *Sci Rep* 2016;6:22373.
[35] Vaudry D, Falluel-Morel A, Bourgault S, et al. Pituitary adenylate cyclase-activating polypeptide and its receptors: 20 years after the discovery. *Pharmacol Rev* 2009;61(3):283–357.
[36] Zhao Wei SG. Conversion of drug dosage among different experimental animals. *Chin J Anim Husb Vet Med* 2010(5): 52–53.
[37] Zazuli Z, Kos R, Veltman JD, et al. Comparison of myelotoxicity and nephrotoxicity between daily low-dose cisplatin with concurrent radiation and cyclic high-dose cisplatin in non-small cell lung cancer patients. *Front Pharmacol* 2020;11:975.
[38] Kerbel RS, Kamen BA. The anti-angiogenic basis of metronomic chemotherapy. *Nat Rev Cancer* 2004;4(6):423–436.
[39] Xing JJ, Mi XJ, Hou JG, et al. Maltol mitigates cisplatin-evoked cardiotoxicity via inhibiting the PI3K/Akt signaling pathway in rodents in vivo and in vitro. *Phytother Res* 2022;36(4):1724–1735.
[40] Mao N, Wu X, Wang C, et al. Effect of moxibustion combined with cisplatin on tumor microenvironment hypoxia and vascular normalization in Lewis lung cancer mice. *Integr Cancer Ther* 2023;22:15347354231198195.
[41] Han JS. Acupuncture: neuropeptide release produced by electrical stimulation of different frequencies. *Trends Neurosci* 2003;26(1):17–22.
[42] Daenen LG, Roodhart JM, van Amersfoort M, et al. Chemotherapy enhances metastasis formation via VEGFR-1-expressing endothelial cells. *Cancer Res* 2011;71(22):6976–6985.
[43] Kim R, An M, Lee H, et al. Early tumor-immune microenvironmental remodeling and response to first-line fluoropyrimidine and platinum chemotherapy in advanced gastric cancer. *Cancer Discov* 2022;12(4):984–1001.
[44] Dijkgraaf EM, Heusinkveld M, Tummers B, et al. Chemotherapy alters monocyte differentiation to favor generation of cancer-supporting M2 macrophages in the tumor microenvironment. *Cancer Res* 2013;73(8):2480–2492.
[45] Yang Y, Wu M, Cao D, et al. ZBP1-MLKL necroptotic signaling potentiates radiation-induced antitumor immunity via intratumoral STING pathway activation. *Sci Adv* 2021;7(41):eabf6290.
[46] Li X, Wu XQ, Deng R, et al. CaMKII-mediated Beclin 1 phosphorylation regulates autophagy that promotes degradation of Id and neuroblastoma cell differentiation. *Nat Commun* 2017;8(1):1159.
[47] Dangaj D, Bruand M, Grimm AJ, et al. Cooperation between constitutive and inducible chemokines enables T cell engraftment and immune attack in solid tumors. *Cancer Cell* 2019;35(6):885–900. e10.
[48] Liu X, Hogg GD, Zuo C, et al. Context-dependent activation of STING-interferon signaling by CD11b agonists enhances anti-tumor immunity. *Cancer Cell* 2023;41(6):1073–1090.e12.
[49] Müller E, Speth M, Christopoulos PF, et al. Both type I and type II interferons can activate antitumor M1 macrophages when combined with TLR stimulation. *Front Immunol* 2018;9:2520.
[50] Morante-Palacios O, Fondelli F, Ballestar E, et al. Tolerogenic dendritic cells in autoimmunity and inflammatory diseases. *Trends Immunol* 2021;42(1):59–75.
[51] Knochelmann HM, Dwyer CJ, Bailey SR, et al. When worlds collide: Th17 and Treg cells in cancer and autoimmunity. *Cell Mol Immunol* 2018;15(5):458–469.
[52] Hoe E, Anderson J, Nathanielsz J, et al. The contrasting roles of Th17 immunity in human health and disease. *Microbiol Immunol* 2017;61(2):49–56.
[53] Dighe AS, Richards E, Old LJ, et al. Enhanced in vivo growth and resistance to rejection of tumor cells expressing dominant negative IFN gamma receptors. *Immunity* 1994;1(6):447–456.
[54] Kaplan DH, Shankaran V, Dighe AS, et al. Demonstration of an interferon gamma-dependent tumor surveillance system in immunocompetent mice. *Proc Natl Acad Sci U S A* 1998;95(13):7556–7561.

[55] Joshi S, Sharabi A. Targeting myeloid-derived suppressor cells to enhance natural killer cell-based immunotherapy. *Pharmacol Ther* 2022;235:108114.
[56] Hiam-Galvez KJ, Allen BM, Spitzer MH. Systemic immunity in cancer. *Nat Rev Cancer* 2021;21(6):345–359.
[57] Xu L, Zou C, Zhang S, et al. Reshaping the systemic tumor immune environment (STIE) and tumor immune microenvironment (TIME) to enhance immunotherapy efficacy in solid tumors. *J Hematol Oncol* 2022;15(1):87.
[58] Van C, Condro MC, Lov K, et al. PACAP/PAC1 regulation of inflammation via catecholaminergic neurons in a model of multiple sclerosis. *J Mol Neurosci* 2019;68(3):439–451.
[59] Maugeri G, D'Amico AG, Reitano R, et al. PACAP and VIP inhibit the invasiveness of glioblastoma cells exposed to hypoxia through the regulation of HIFs and EGFR expression. *Front Pharmacol* 2016;7:139.
[60] Maugeri G, D'Amico AG, Saccone S, et al. Effect of PACAP on hypoxia-induced angiogenesis and epithelial-mesenchymal transition in glioblastoma. *Biomedicines* 2021;9(8):965.
[61] Chang X, Lu T, Huang J. Preliminary study on microvasculature normalization induced by peritumoral electroacupuncture in mice with breast cancer xenografts. *Sichuan Da Xue Xue Bao Yi Xue Ban* 2023;54(5):972–977.
[62] Chang X, Zhu Y, Zhao W, et al. Electro-acupuncture for health-related quality of life and symptoms in patients with gastric cancer undergoing adjuvant chemotherapy (EAGER): a protocol for a multicenter randomized controlled trial. *Health Qual Life Outcomes* 2023;21(1):70.
[63] Chan K, Lui L, Yu K, et al. The efficacy and safety of electro-acupuncture for alleviating chemotherapy-induced peripheral neuropathy in patients with coloreactal cancer: study protocol for a single-blinded, randomized sham-controlled trial. *Trials* 2020;21(1):58.
[64] Yue H, Zhou S, Wu H, et al. Efficacy and safety of electro-acupuncture (EA) on insomnia in patients with lung cancer: study protocol of a randomized controlled trial. *Trials* 2020;21(1):788.
[65] Garland SN, Xie SX, Li Q, et al. Comparative effectiveness of electro-acupuncture versus gabapentin for sleep disturbances in breast cancer survivors with hot flashes: a randomized trial. *Menopause* 2017;24(5):517–523.
[66] Bao T, Zhi WI, Baser RE, et al. Electro-acupuncture versus battle field auricular acupuncture in breast cancer survivors with chronic musculoskeletal pain: subgroup analysis of a randomized clinical trial. *Breast Cancer Res Treat* 2023;202(2):287–295.